ARTICLES
PUBLISHED ONLINE: 31 MARCH 2009 | DOI: 10.1038/NGEO473
nature geoscience

# Climate response to regional radiative forcing during the twentieth century

Drew Shindell* and Greg Faluvegi

**Regional climate change can arise from three different effects: regional changes to the amount of radiative heating that reaches the Earth's surface, an inhomogeneous response to globally uniform changes in radiative heating and variability without a specific forcing. The relative importance of these effects is not clear, particularly because neither the response to regional forcings nor the regional forcings themselves are well known for the twentieth century. Here we investigate the sensitivity of regional climate to changes in carbon dioxide, black carbon aerosols, sulphate aerosols and ozone in the tropics, mid-latitudes and polar regions, using a coupled ocean–atmosphere model. We find that mid- and high-latitude climate is quite sensitive to the location of the forcing. Using these relationships between forcing and response along with observations of twentieth century climate change, we reconstruct radiative forcing from aerosols in space and time. Our reconstructions broadly agree with historical emissions estimates, and can explain the differences between observed changes in Arctic temperatures and expectations from non-aerosol forcings plus unforced variability. We conclude that decreasing concentrations of sulphate aerosols and increasing concentrations of black carbon have substantially contributed to rapid Arctic warming during the past three decades.**

Both detection and attribution studies and climate models have examined the surface temperature response to spatially variable radiative forcing, but for radiative forcing taking place simultaneously over much of the world (for example, pre-industrial to present-day aerosol changes) rather than investigating the response to forcing in a particular location. Such studies indicate that at continental scales, responses are not closely correlated with radiative forcing, but instead broadly match the response to more homogeneous forcings such as well-mixed greenhouse gases[1–4] (WMGHGs). At hemispheric scales, however, the radiative forcing location influences the response, and the space–time patterns of twentieth century hemispheric surface temperature changes have been used to infer the Northern Hemisphere influence of sulphate aerosols[5–7]. Nonetheless, how the response at different spatial scales depends on the radiative forcing location remains unclear, as do the regional forcings themselves[8–14]. Here we systematically investigate the sensitivity of regional climate to location and type of forcing. We demonstrate that the mean tropical surface temperature response, like the global mean, shows relatively weak sensitivity to forcing location. In contrast, the extratropics are much more sensitive to local forcings, with reduced response to forcing in the tropics and especially the opposite hemisphere. Observed twentieth century surface temperatures are consistent with these findings, with tropical temperatures following the global mean but substantial departures in the extratropics. Hence, global and tropical mean temperature trends during the twentieth century would have been quite similar if short-lived-species radiative forcing had been distributed homogeneously rather than being concentrated in the northern extratropics. Regional concentration of forcing contributed to the departures of Northern Hemisphere mid-latitude (NHml) and Arctic temperature trends from the global or Southern Hemisphere extratopical (SHext) means, however. We then compare observed global mean and meridional gradients in surface temperature with internal variability and the response to homogeneous forcings and ozone in climate models, and show that these factors alone cannot fully account for the observations. Finally, using inverse methods we derive the aerosol forcing required to explain the observations. Whereas earlier studies used similar methods to derive total aerosol forcing, we use the regional forcing/response relationships calculated here to derive regional values and compare with historical emissions to estimate contributions by particular species. Hence, we provide a much more complete estimate of the space–time aerosol forcings by region and aerosol type.

## Climate modelling of response to regional forcing

We present surface temperature responses over broad latitude bands to changes in WMGHGs, ozone and aerosols (see the Methods section). Global mean temperatures follow the global mean radiative forcing fairly closely (Fig. 1a), with ~45% enhancement for extratropical relative to tropical $CO_2$ forcing (comparable to other studies[15]) owing to strong climate feedbacks at higher latitudes. Global mean sensitivity to tropical and NHml sulphate is similar to that for $CO_2$, but the high-latitude sensitivity is ~50% greater than for tropical forcing with aerosol indirect effects (AIEs). However, it is ~75% less without AIE because the direct impact of reflective sulphate is reduced over highly reflective surfaces.

Tropical, mid-latitude or polar mean temperatures largely follow the forcing per local unit area when the forcing is applied within that latitude band (Fig. 1d,f,h,j). Imposing equivalent global mean radiative forcing requires more local forcing as the area within the band decreases, so that mid-latitude forcing must be ~2.4 times larger than tropical forcing and polar forcing must be ~7 times greater. This accounts for increased sensitivity to higher latitude forcings when examining response per global mean radiative forcing (Fig. 1c,e,i).

Tropical mean temperatures generally follow the global mean forcing regardless of forcing location (Fig. 1g; all responses near dashed line), although the response is enhanced (~40%) for local forcings. For other regions, however, the response to non-local forcings is not proportional to the global mean forcing (Fig. 1c,e,i; responses deviate greatly from dashed line). Extratropical regions

NASA Goddard Institute for Space Studies (GISS) and Columbia University, New York 10025, USA. *e-mail: Drew.T.Shindell@nasa.gov.

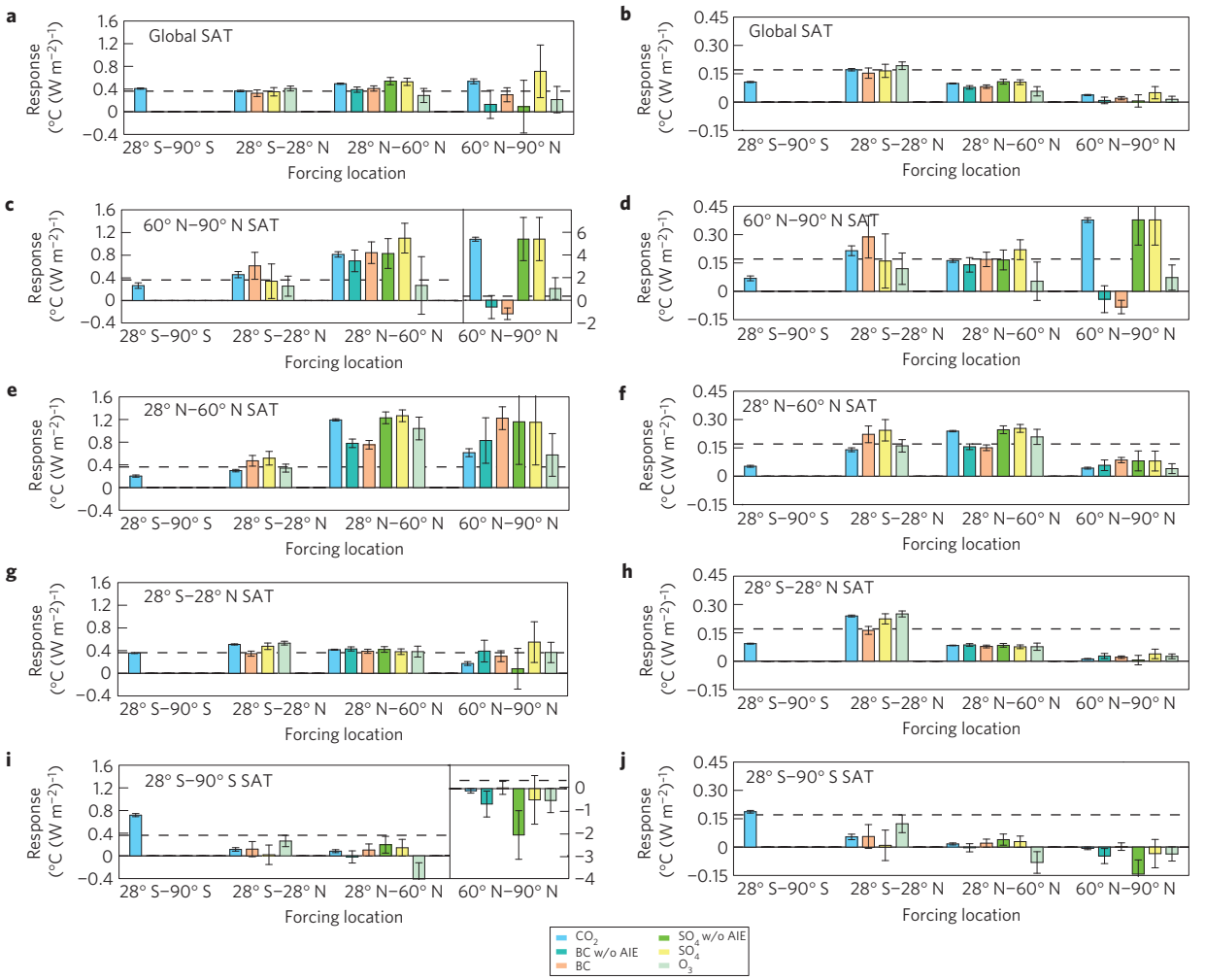


**Figure 1 | Regional climate response to forcing applied in various latitude bands.** The rows show surface air temperature (SAT) changes in the region indicated in the upper left corner, with the response shown as the SAT change per unit positive global (left column) or local (right column) radiative forcing. The colours indicate the type of forcing applied (see legend; BC: black carbon), and the band in which the forcing was applied is given on the *x* axis. Radiative forcing is the mean annual-average adjusted value at the tropopause and SAT is the area-weighted mean. Global mean responses to tropical forcing (0.36 °C (global W m$^{-2}$)$^{-1}$ and 0.17 °C (local W m$^{-2}$)$^{-1}$) are shown in all rows (dashed line) for comparison. Uncertainties are standard deviations in 80-year equilibrium runs.

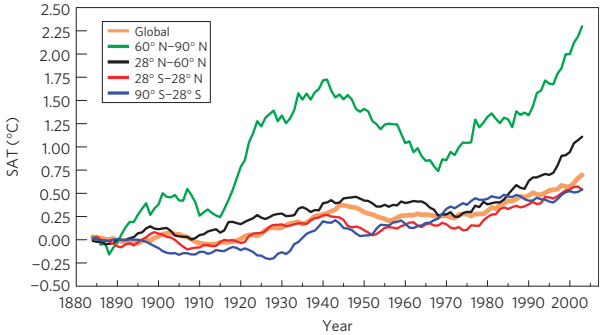


**Figure 2 | Area-weighted mean observed surface temperatures[39,40] over the indicated latitude bands.** The values are nine-year running means relative to the 1880–1890 mean. Correlations ($R^2$) with the global mean over 1931–2007 by region are: 0.94 tropics, 0.61 SHext, 0.86 NHml and 0.53 Arctic.

typically show decreasing responses as the forcing becomes more remote (Fig. 1d,f,j). Hence, 1 W m$^{-2}$ tropical forcing causes a similar extratropical response as 1 W m$^{-2}$ extratropical forcing despite the tropical forcing being imposed over twice as much area, whereas 1 W m$^{-2}$ forcing in the opposite hemisphere induces relatively little response. This suggests that heat fluxes can transfer some of the influence of forcings between the tropics and extratropics, but transfer little between the extratropical zones. Hence, uneven forcing distributions have little effect on global or tropical climate responses, but can profoundly affect extratropical responses.

Enhanced regional sensitivities to local forcings at higher latitudes (Fig. 1d) can be understood through regional energy budgets (see Supplementary Note). These demonstrate that local cloud, water vapour and surface albedo feedbacks are responsible for the greater global and local sensitivities to extratropical forcing. In the Arctic, surface climate response also depends strongly on the type of forcing imposed (Fig. 1d). This results from a reduction in poleward heat flux following local heating by absorbing aerosols or ozone.

## Evaluating the historical record

We now compare the historical patterns of space–time surface temperature (Fig. 2) with responses to WMGHGs, natural forcings and ozone. Given the distinct spatial patterns of climate response to

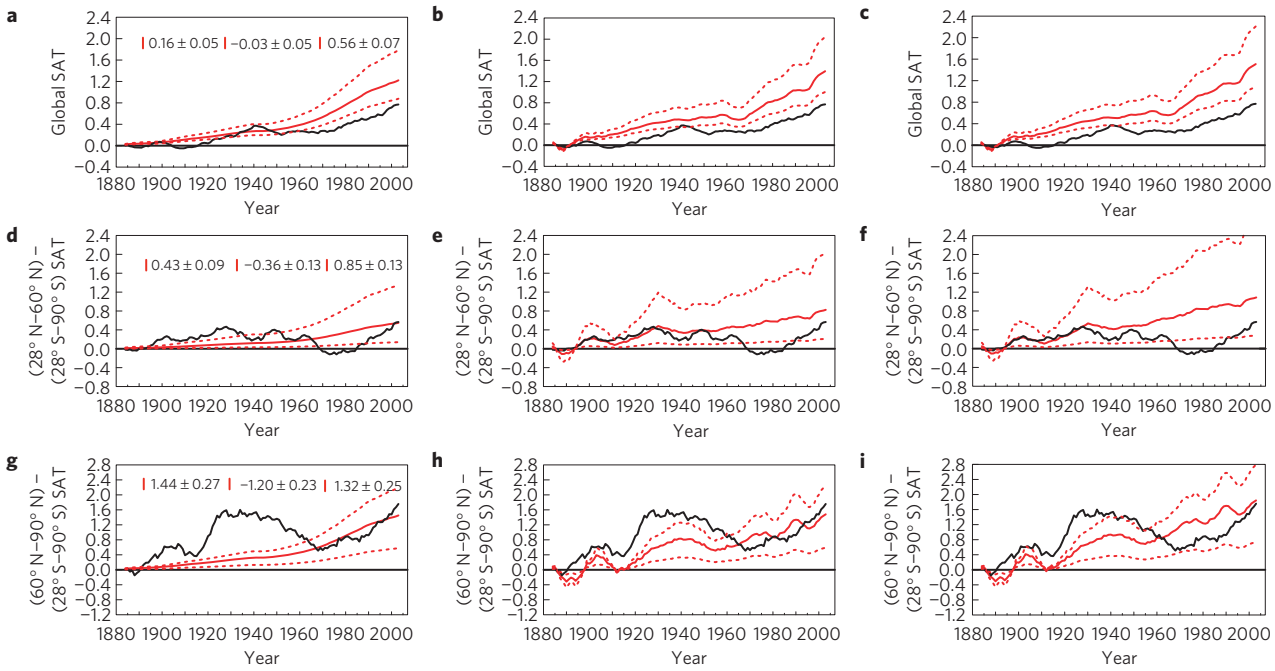


**Figure 3 | Time evolution of observed (black; nine-year running mean) surface temperatures and values reconstructed from models.** The red solid lines indicate the mean reconstructed CMIP3 global or gradient response and dashed lines are the maximum and minimum responses. The columns show the response to WMGHGs (G; left), to WMGHGs plus natural forcings (G+N; centre) and those forcings plus ozone changes (G+N+O; right). Numerical values for observed linear trends during 1890–1930, 1931–1975 and 1976–2007 are given in the left column (observed Arctic trends for the three time periods are: 1.25±0.25, −0.86±0.23 and 1.48±0.28 °C).

regional forcings, we can then carry out inverse calculations of extra forcing required to account for any residuals.

We first examine the global and NHml–SHext gradient responses to increasing $CO_2$. These depart substantially from one another in observations (Fig. 3a,d). Responses are reconstructed by multiplying the WMGHG radiative forcing time series by the response per unit forcing in Coupled Model Intercomparison Project phase 3 (CMIP3) simulations (see the Methods section). Different model sensitivities scale the amplitude of the reconstructed time series, creating a large range of model responses (Fig. 3a,d), but the shapes are fixed by the well-constrained radiative forcing time series. Mismatches in multi-decadal trends are substantial for all models, with the timing of greatest disagreement depending on the gradient response per unit forcing. The models similarly fail to capture the time evolution of Arctic–SHext gradients (Fig. 3g).

The effects of other forcings were not isolated in CMIP3. However, a model intercomparison of the response to global and regional WMGHG, solar and ozone forcing indicates that the dominant source of variations in the zonal mean response is the underlying climate model rather than the forcing agent[16]. Consistent with this, regional responses to equivalent $CO_2$, ozone or sulphate forcing are quite similar in our model (outside the polar regions: Fig. 1). Thus, a model's regional sensitivity to $CO_2$ seems to reliably indicate its response in that region to other forcings. Hence, we reconstruct the response to solar, volcanic and ozone forcing using the range of CMIP3 $CO_2$ sensitivities to characterize the range of physical processes that would be expected to underlie the uncertainty in response to those forcings. We also include uncertainties in the forcings themselves (see the Methods section). Notably, the multimodel mean response to WMGHGs plus natural forcing (G + N; Fig. 3b,e,h) does a better job of capturing the observed NHml–SHext gradient during the early twentieth century than the response to WMGHGs alone. The addition of ozone forcing minimally affects early twentieth century gradients, but increases the trends in gradients during later periods (Fig. 3c,f,i).

Observed gradients show three distinct phases, with the NHml and Arctic warming more than the SHext until ~1930, less (or even cooling) from ~1931–1975 and again warming more rapidly thereafter (Fig. 3). The G+N+O reconstructed responses cannot capture the negative NHml–SHext or Arctic–SHext trends during 1931–1975, the subsequent rapid increase in the NHml–SHext gradient or the 1880–1930 increase in the Arctic–SHext gradient. Slopes of reconstructed 1976–2007 trends are generally consistent only for high gradient sensitivities, which show the greatest inconsistencies during 1931–1975.

## Inferred aerosol forcings and internal variability

Differences between observed and reconstructed G+N+O global means and gradients are probably attributable to internal variability and aerosol forcings, which are poorly constrained from forward modelling or observations[8–10]. Using our regional forcing/response relationships, we derive the aerosol forcings that best account for these differences and compare their impact with internal variability in coupled model control runs (see the Methods section). Our 1890–2007 global mean net aerosol radiative forcing is $-1.31 \pm 0.52\,W\,m^{-2}$, a value consistent with recent estimates[13] of $-1.2\,W\,m^{-2}$ (probable range $-2.4$ to $-0.6\,W\,m^{-2}$). Distinct regional aerosol forcings are required to match both the observed global mean and regional gradient trends.

During 1890–1930, substantial global mean cooling is required to bring the G + N + O trend down to the observations (Fig. 4a). Although internal variability might contribute to this cooling, all of the models require extra cooling from aerosols. G + N + O forcing largely captures the observed 1890–1930 NHml–SHext temperature gradient trend for most models; hence, the aerosol forcing must minimally affect that gradient. As tropical forcing affects the NHml more than the SHext (Fig. 1f versus j), positive NHml forcing is typically required to keep the NHml–SHext gradient from decreasing in the face of negative tropical forcing required for global mean cooling (Fig. 4d). Several

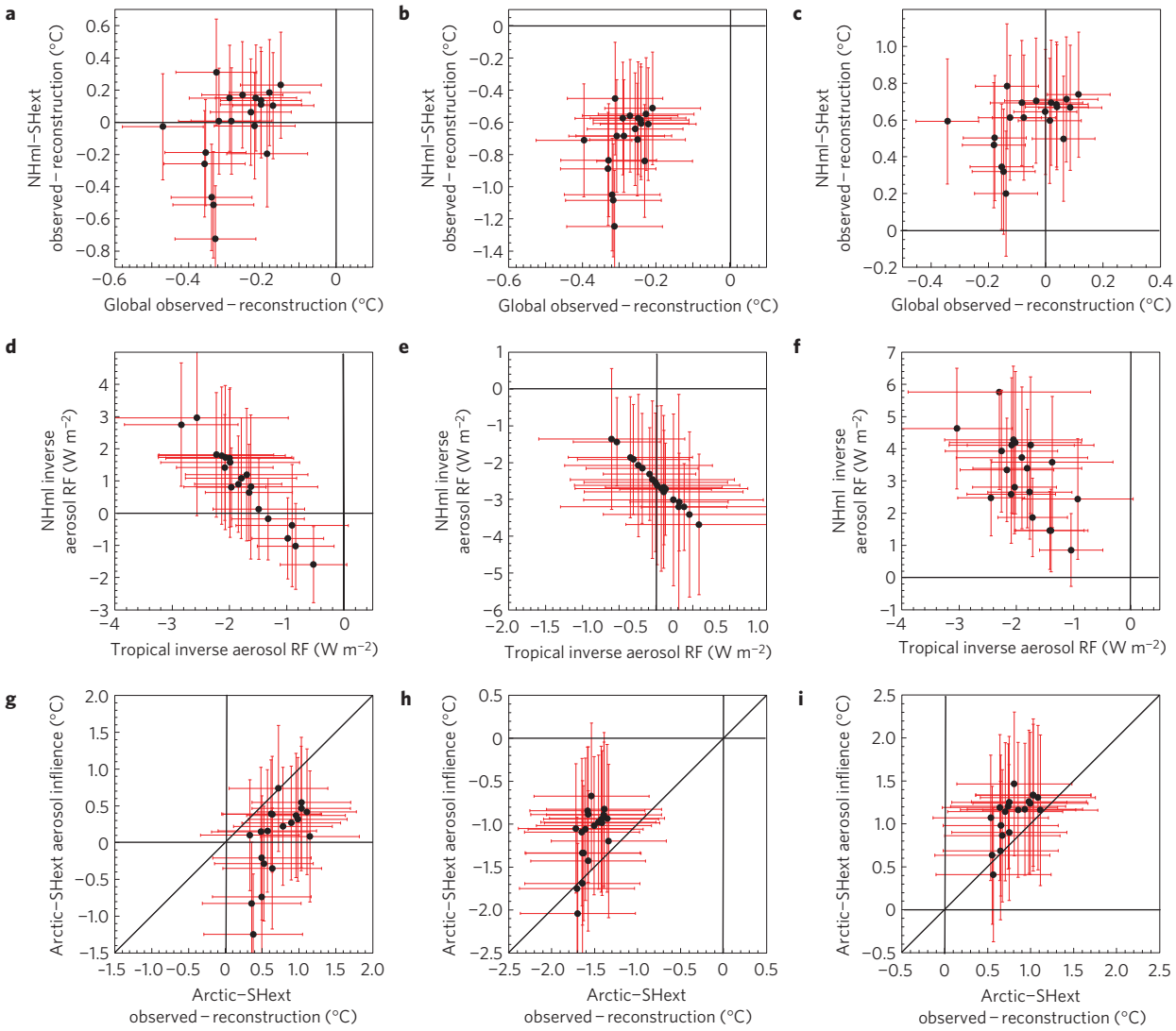


**Figure 4 | Global mean and regional gradient surface temperature trends derived from observations and models and aerosol forcing estimates.** The first row shows observations minus the reconstructed influence of WMGHG + natural + ozone (G + N + O) forcing. The second row shows the regional aerosol forcings (per unit local area) required to match the first row's constraints. RF: radiative forcing. The third row shows observations minus the reconstructed G + N + O Arctic–SHext gradient compared with the aerosol impact on that gradient. The columns show 1890–1930 (left), 1931–1975 (centre) and 1976–2007 (right). The symbols represent calculations using sensitivities (global mean and regional gradients) from 20 climate models. Uncertainties include internal variability, natural and ozone forcing uncertainties and uncertainty in observed trend calculations.

models overestimate the NHml–SHext gradient trend in response to G + N + O forcing (Fig. 4a), and hence require negative NHml aerosol forcing. Results are nearly always consistent with zero NHml aerosol forcing, however, given the influence of internal variability.

Internal variability alone is not sufficient to reconcile either the G + N + O global mean or NHml–SHext trends with observations during the 1931–1975 period (Fig. 4b). To match the observations, negative NHml aerosol forcing is required, whereas possible tropical forcings are small values of either sign consistent with no tropical forcing (Fig. 4e).

The past three decades show the most rapid increase in both global mean and NHml–SHext temperatures (Fig. 3). Some models are consistent with either the global mean or the NHml–SHext trend during this period including G + N + O forcing and internal variability, but none is consistent with both (Fig. 4c). During 1976–2007, reproducing the NHml–SHext gradient requires large positive NHml forcing in most models, and matching global mean temperatures then requires negative tropical forcing (Fig. 4f). Hence, all models require aerosol forcing, but the tropical to mid-latitude ratio varies substantially.

**Comparison with historical emissions** Inferred aerosol forcings are in general qualitatively consistent with historical emissions. Sulphate aerosol precursor emissions from anthropogenic activities increased roughly fourfold from 1880 to the 1920s, almost all at NHmls, and increased roughly 3.5 times from the 1920s to the 1970s, primarily at NHmls but also in the tropics, whereas since then NHml emissions decreased rapidly and tropical emissions increased[17]. Black carbon emissions from biofuel and fossil-fuel combustion increased ~50% from 1880 to the 1920s, nearly all from NHmls, rose ~25% from the 1920s to the 1970s, primarily in the tropics, then rose ~30% from the 1970s to 2000, with both tropical and NHml emissions increasing[18].

The inferred positive 1976–2007 NHml aerosol forcing is consistent with simultaneously increasing black carbon and decreasing sulphate, whereas the negative tropical forcing could reasonably result from increased sulphate outweighing increased

black carbon. During 1931–1975, the negative NHml forcing is consistent with large sulphate increases and constant black carbon, whereas the small tropical forcing is consistent with near-balance between increased sulphate and black carbon. The 1890–1930 forcings are less clearly aligned with historical emissions estimates. Both black carbon and sulphur dioxide emissions at NHml increased during this time. Depending on the relative importance of these two, forcing might plausibly be either positive or negative. Inferred tropical aerosol forcing values are all negative, but the larger values would match emissions only if strong nonlinearities made the small emission increases during this time especially effective in causing negative forcing. This is possible, however, as the AIE dependence on cloud droplet number is logarithmic[19].

In addition, historical emissions from biomass burning are poorly known. These might have increased substantially during 1890–1930, with tropical emissions having an especially large impact due to the relative lack of tropical background terrestrial aerosol emissions. Temperature observations in the early period are also limited in spatial coverage (see Supplementary Fig. S2), which could bias early trends. Further work on this early time period is clearly necessary. During the 1931–1975 and 1976–2007 intervals, however, the inferred aerosol forcings seem qualitatively consistent with historical emissions (as well as with limited available surface radiation flux measurements[20]). Quantitative comparison will require improved understanding of aerosol physical and chemical processes.

## Evaluation of independent Arctic–SHext gradients

We further test the inverse results by examining their impact on the Arctic (60°–90° N) minus SHext gradient. As trends in this gradient result primarily from Arctic temperatures (Fig. 3), they provide a largely independent test of our aerosol forcings. We include aerosol direct forcing, AIE and the influence of black carbon deposition (see Supplementary Methods).

During 1890–1930, the Arctic–SHext gradient increased markedly (1.4 °C; Fig. 3g). The modelled response to G + N + O accounts for ~20–70% of the increase (Fig. 3i). Internal variability can account for the remainder in several models (horizontal error bars in Fig. 4g overlap zero), but not in most. The combined influence of aerosols and internal variability (vertical error bars in Fig. 4g, which include internal variability elsewhere that influences inverse aerosol forcings) can account for the observations − G + N + O reconstruction difference within the 95% confidence limits in most models because the inferred aerosol forcing usually increases this gradient. For those few models with very sensitive NHml–SHext gradients, which led to quite negative NHml–SHext observations − G + N + O reconstructed trends (Fig. 4a), the negative aerosol forcings decrease the Arctic–SHext gradient significantly (Fig. 4g). Hence, these three models cannot reproduce both the observed global mean and regional gradient trends using our forcing/response relationships and internal variability.

From 1931–1975, the observed Arctic–SHext gradient decreased, but G + N + O forcings increased this gradient (Fig. 3i), resulting in a trend overestimate of ~1.4–1.7 °C. The effects of our inferred aerosol forcings account for this difference in every model, and internal variability alone accounts for at most half the overestimate (Fig. 4h). From 1976–2007, G + N + O forcing accounts for ~30–60% of the observed gradient increase of 1.3 °C. The inferred aerosol impacts are consistent with the remainder in all models, although 3 of the 20 models are consistent with both no aerosol impact on the Arctic and no residual between observations and the reconstructed influence of non-aerosol forcings plus internal variability (although these are the same 3 that show very large discrepancies during 1890–1930).

## Historical and future climate change due to regional forcing

The hemispheric asymmetry of observed temperature trends and some aspects of their regional spatial structure have been linked to aerosols in detection and attribution studies[6,7,21]. Several previous studies have carried out inverse estimates using global and regional temperature differences to derive global sulphate aerosol forcings[5,7,22]. Our study finds results consistent with the earlier analyses for twentieth century global net aerosol radiative forcing, and adds calculations of regional aerosol forcing during specific time intervals. Combined with historical emissions, the inferred net radiative forcings are linked to reflective and absorbing aerosol changes.

Projected climate change patterns are thought to often be independent of the particular scenario and forcings[1,2,4,23]. Here we show that Arctic and mid-latitude climate change is in fact sensitive to the distribution of aerosols and tropospheric ozone. Hence, 'pattern scaling' using the global response to global forcing is unlikely to provide realistic results for alternative short-lived-species emission scenarios. Furthermore, many current projections that do not include black carbon and tropospheric ozone changes[23] may have substantial regional biases.

## Aerosol influence on recent climate and the Arctic

Our results suggest that aerosols have had a large role in both global and regional climate change during the twentieth century. Both these results and forward modelling[24–26] indicate that Arctic climate is especially sensitive to Northern Hemisphere short-lived pollutants. Arctic trends may also be related to internal atmosphere–ocean dynamics[27–29]. Our analysis is consistent with a large role for internal variability, but suggests an even greater impact from aerosol forcing on trends since 1930. A large aerosol contribution to mid-twentieth century Arctic cooling perhaps accounts for the lack of polar amplification in some studies[30]. During 1976–2007, we estimate that aerosols contributed 1.09 ± 0.81 °C to the observed Arctic surface temperature increase of 1.48 ± 0.28 °C. Hence, much of this warming may stem from the unintended consequences of clean-air policies that have greatly decreased sulphate precursor emissions from North America and Europe (reducing the sulphate masking of greenhouse warming) and from large increases in Asian black carbon emissions.

Current understanding of AIE under Arctic conditions is quite limited[24]. Hence, Arctic AIE is included only crudely here. However, our results indicate that the net impact on 1890–2007 Arctic surface temperatures has been −0.6 °C from tropical aerosols, +0.4 °C from mid-latitude aerosols and +0.5 °C from Arctic aerosols. Hence, long-term aerosol-induced Arctic climate change is quite sensitive to forcing at lower latitudes[31], which is not subject to these uncertainties. During 1976–2007, however, large changes in mid-latitude emissions have increased the importance of local Arctic forcing, with estimated surface temperature changes of −0.3 °C from tropical aerosols, +0.6 °C from mid-latitude aerosols and +0.8 °C from Arctic aerosols during this time. It is thus important to better understand AIE under Arctic conditions.

Our calculations suggest that black carbon and tropospheric ozone have contributed ~0.5–1.4 °C and ~0.2–0.4 °C, respectively, to Arctic warming since 1890, making them attractive targets for Arctic warming mitigation. In addition, they respond quickly to emissions controls, and reductions have ancillary benefits including improved human and ecosystem health[32].

## Methods

**Modelling of regional forcing/response relationships.** We carried out equilibrium climate simulations with the coupled atmosphere–ocean climate model GISS-ER (ref. 33), examining the response to individual forcings imposed over the tropics (28° S–28° N), mid-latitudes (28°–60°) and the polar regions (60°–90°), bands that have generally faster atmospheric mixing within them than across their boundaries[34,35], and hence where regional emissions of short-lived species and their

precursors have their greatest impact on radiative forcing. The forcings used were increases in $CO_2$ (representative of the WMGHGs) and black carbon and decreases in sulphate (representative of reflective aerosols) and ozone. Carbon dioxide was scaled uniformly over the band, whereas aerosol and ozone forcings were imposed by perturbing present-day distributions by a constant factor. Hence, these latter forcings have a spatial structure comparable to historical changes. Simulations were integrated for 120 years, with analysis using area-weighted means over the past 80 years following stabilization of the climate. Initial conditions are from a 900-year control run with this model. Aerosol perturbation experiments were run both with and without a simple parameterization for the AIE (see Supplementary Methods for further details).

**Analysis of the historical record.** We reconstructed responses to WMGHG, solar, volcanic and ozone forcings to compare with observations. For WMGHGs, we examined the transient response to 1% $yr^{-1}$ $CO_2$ increases in CMIP3 simulations. We calculated linear trends in global and zonal mean temperature over the period up to doubling of $CO_2$ in 20 climate models. We then calculated the transient global mean temperature and temperature gradient responses per unit radiative forcing by dividing by the radiative forcing calculated in individual CMIP3 models for the nine models for which this is available[36] and otherwise using the mean radiative forcing from those nine. These normalized responses are multiplied by the total WMGHG radiative forcing time series derived from observed gas abundances to obtain time-evolving responses to increasing WMGHGs from all 20 models (see Supplementary Methods for further details).

As noted, previous studies indicate that variations between model responses are much greater than the variation in response to different forcings in a single model, and that the zonal mean sensitivities to global $CO_2$ forcing in models are a fairly good predictor of sensitivity to regional forcing[16]. Hence, the solar response is reconstructed by multiplying CMIP3 global and regional responses per unit forcing by the solar radiative forcing time series[37], as with WMGHGs. For inhomogeneous volcanic and ozone forcing, we use the time-dependent responses averaged over five-member ensembles of GISS-ER 1880–2003 simulations[38]. For the volcanic ensemble, we apply a nine-year running mean to capture decadal timescale trends rather than the strong response immediately following eruptions. Responses to volcanism and ozone are then scaled by the ratio of the global or regional response in a given CMIP3 model to that seen in the GISS-ER CMIP3 run to obtain the reconstructed responses (equations given in Supplementary Methods). Hence, the spatial and temporal patterns of the GISS response inform the reconstruction, but the scaling allows the spatial pattern and global mean to change according to each model's sensitivity.

To quantify internal variability, we examined 30–45-year segments of a 1,150-year control run of the GISS-ER climate model and shorter CMIP3 controls of other models (see Supplementary Methods). We also assumed that the magnitudes of natural and ozone radiative forcings are uncertain by a factor of two. Overall uncertainties for a given CMIP3 model's reconstructed global mean or gradient change versus observations are given as the sum in quadrature of internal variability, the uncertainty in forcings and the standard error from the linear regression calculation of observed trends. 95% confidence levels are used throughout this work.

**Inferred aerosol forcings.** Using global temperatures and NHml–SHext gradients, we solve for the NHml and tropical forcing during each of the three time periods discussed previously that accounts for the difference between observations and G+N+O reconstructions (see Supplementary Methods for further details). Aerosol responses are normalized by the ratio of transient to equilibrium responses seen in our $CO_2$ simulations (0.80). We include the effects of black carbon deposition in the Arctic, on the basis of previous GISS modelling of pre-industrial to present-day changes, in the calculation. Inferred values are net radiative forcing rather than forcing by individual species. Uncertainties are dominated by the influence of internal variability.

Forcing–response relationships for aerosols have not yet been derived for multiple models. However, in the GISS model, sensitivity to aerosols is very similar to that for WMGHGs (outside the polar regions) (Fig. 1). Hence, as with ozone and volcanic forcing, we scale the GISS model responses by the ratio of regional response to $CO_2$ in CMIP3 models versus GISS-ER to characterize the possible responses to aerosol forcing. Experiments with multiple climate models explicitly examining the sensitivity to regional aerosol forcing would be useful to better constrain this portion of the inverse calculation.

Received 1 September 2008; accepted 25 February 2009; published online 31 March 2009

## References


1. Boer, G. & Yu, B. Climate sensitivity and response. *Clim. Dyn.* **20**, 415–429 (2003).
2. Hansen, J. *et al.* Efficacy of climate forcings. *J. Geophys. Res.* **110**, D18104 (2005).
3. Mitchell, J. F. B., Davis, R. A., Ingram, W. J. & Senior, C. A. On surface temperature, greenhouse gases, and aerosols: Models and observations. *J. Clim.* **8**, 2364–2386 (1995).
4. Shindell, D. T. *et al.* Multi-model projections of climate change from short-lived emissions due to human activities. *J. Geophys. Res.* **113**, D11109 (2008).
5. Andronova, N. G. & Schlesinger, M. E. Objective estimation of the probability density function for climate sensitivity. *J. Geophys. Res.* **106**, 22605–22611 (2001).
6. Santer, B. D. *et al.* A search for human influences on the thermal structure of the atmosphere. *Nature* **382**, 39–46 (1996).
7. Stott, P. A. *et al.* Observational constraints on past attributable warming and predictions of future global warming. *J. Clim.* **19**, 3055–3069 (2006).
8. Schulz, M. *et al.* Radiative forcing by aerosols as derived from the AeroCom present-day and pre-industrial simulations. *Atmos. Chem. Phys.* **6**, 5225–5246 (2006).
9. Bellouin, N., Boucher, O., Haywood, J. & Reddy, M. S. Global estimate of aerosol direct radiative forcing from satellite measurements. *Nature* **438**, 1138–1141 (2005).
10. Chung, C. E., Ramanathan, V., Kim, D. & Podgorny, I. A. Global anthropogenic aerosol direct forcing derived from satellite and ground-based observations. *J. Geophys. Res.* **110**, D24207 (2005).
11. Mickley, L. J., Jacob, D. J. & Rind, D. Uncertainty in preindustrial abundance of tropospheric ozone: Implications for radiative forcing calculations. *J. Geophys. Res.* **106**, 3389–3399 (2001).
12. Shindell, D. T. & Faluvegi, G. An exploration of ozone changes and their radiative forcing before the chlorofluorocarbon era. *Atmos. Chem. Phys.* **2**, 363–374 (2002).
13. Forster, P. *et al.* in *Climate Change 2007: The Physical Science Basis* (eds Solomon, S. *et al.*) (Cambridge Univ. Press, 2007).
14. Penner, J. E. *et al.* Model intercomparison of indirect aerosol effects. *Atmos. Chem. Phys.* **6**, 3391–3405 (2006).
15. Forster, P. M. d. F., Blackburn, M., Glover, R. & Shine, K. P. An examination of climate sensitivity for idealised climate change experiments in an intermediate general circulation model. *Clim. Dyn.* **16**, 833–849 (2000).
16. Joshi, M. *et al.* A comparison of climate response to different radiative forcings in three general circulation models: Towards an improved metric of climate change. *Clim. Dyn.* **20**, 843–854 (2003).
17. Smith, S. J., Pitcher, H. & Wigley, T. M. L. Global and regional anthropogenic sulfur dioxide emissions. *Glob. Planet. Change* **29**, 99–119 (2001).
18. Bond, T. C. *et al.* Historical emissions of black and organic carbon aerosol from energy-related combustion, 1850–2000. *Glob. Biogeochem. Cycles* **21**, GB2018 (2007).
19. Gultepe, I. & Isaac, G. A. Scale effects on averaging cloud droplet and aerosol number concentrations: Observations and models. *J. Clim.* **12**, 1268–1279 (1999).
20. Philipona, R., Behrens, K. & Ruckstuhl, C. How declining aerosols and rising greenhouse gases forced rapid warming in Europe since the 1980s. *Geophys. Res. Lett.* **36**, L02806 (2009).
21. Kaufmann, R. K. & Stern, D. I. Cointegration analysis of hemispheric temperature relations. *J. Geophys. Res.* **107**, 4012 (2002).
22. Harvey, L. D. D. & Kaufmann, R. K. Simultaneously constraining climate sensitivity and aerosol radiative forcing. *J. Clim.* **15**, 2837–2861 (2002).
23. Meehl, G. A. *et al.* in *Climate Change 2007: The Physical Science Basis* (eds Solomon, S. *et al.*) (Cambridge Univ. Press, 2007).
24. Quinn, P. K. *et al.* Short-lived pollutants in the Arctic: Their climate impact and possible mitigation strategies. *Atmos. Chem. Phys.* **8**, 1723–1735 (2008).
25. Flanner, M. G., Zender, C. S., Randerson, J. T. & Rasch, P. J. Present-day climate forcing and response from black carbon in snow. *J. Geophys. Res.* **112**, D11202 (2007).
26. Shindell, D. T. *et al.* The role of tropospheric ozone increases in 20th century climate change. *J. Geophys. Res.* **111**, D08302 (2006).
27. Schlesinger, M. E. & Ramankutty, N. An oscillation in the global climate system of period 65–70 years. *Nature* **367**, 723–726 (1994).
28. Johannessen, O. M. *et al.* Arctic climate change: Observed and modeled temperature and sea-ice variability. *Tellus* **56A**, 328–341 (2004).
29. Bengtsson, L., Semenov, V. A. & Johannessen, O. M. The early twentieth-century warming in the Arctic—a possible mechanism. *J. Clim.* **17**, 4045–4057 (2004).
30. Polyakov, I. V. *et al.* Observationally based assessment of polar amplification of global warming. *Geophys. Res. Lett.* **29**, 1878 (2002).
31. Shindell, D. Local and remote contributions to Arctic warming. *Geophys. Res. Lett.* **34**, L14704 (2007).
32. West, J. J., Fiore, A. M., Horowitz, L. W. & Mauzerall, D. L. Global health benefits of mitigating ozone pollution with methane emission controls. *Proc. Natl Acad. Sci.* **103**, 3988–3993 (2006).
33. Schmidt, G. A. *et al.* Present day atmospheric simulations using GISS ModelE: Comparison to in-situ, satellite and reanalysis data. *J. Clim.* **19**, 153–192 (2006).

34. Bowman, K. P. & Erukhimova, T. Comparison of global-scale Langrangian transport properties of the NCEP reanalysis and CCM3. *J. Clim.* **17**, 1135–1146 (2004).
35. Klonecki, A. *et al.* Seasonal changes in the transport of pollutants into the Arctic troposphere-model study. *J. Geophys. Res.* **108**, 8367 (2003).
36. Forster, P. M. & Taylor, K. E. Climate forcings and climate sensitivities diagnosed from coupled climate model integrations. *J. Clim.* **19**, 6181–6194 (2006).
37. Lean, J. Evolution of the sun's spectral irradiance since the Maunder Minimum. *Geophys. Res. Lett.* **27**, 2425–2428 (2000).
38. Hansen, J. *et al.* Climate simulations for 1880–2003 with GISS modelE. *Clim. Dyn.* **29**, 661–696 (2007).
39. Hansen, J. *et al.* A closer look at United States and global surface temperature change. *J. Geophys. Res.* **106**, 23947–23963 (2001).
40. Rayner, N. A. *et al.* Global analyses of sea surface temperature, sea ice, and night marine air temperature since the late nineteenth century. *J. Geophys. Res.* **108**, doi:10.1029/2002JD002670 (2003).

## Acknowledgements

We thank NASA's Atmospheric Chemistry Modeling and Analysis Program for support and R. Reudy and H. Teich for technical assistance. We acknowledge the modelling groups, the Program for Climate Model Diagnosis and Intercomparison and the Working Group on Coupled Modelling for making available the CMIP3 data set, which is supported by the Office of Science, US Department of Energy.

## Author contributions

D.S. conceived and designed the experiments and wrote the paper, G.F. carried out the model simulations and both analysed the data.

## Additional information

Supplementary Information accompanies this paper on www.nature.com/naturegeoscience. Reprints and permissions information is available online at http://npg.nature.com/reprintsandpermissions. Correspondence and requests for materials should be addressed to D.S.